The effect of nonpolar solvents on Rydberg states: van der Waals complexes of azabicyclooctanes

Q. Y. Shang, P. O. Moreno, C. Dion, and E. R. Bernstein

Citation: The Journal of Chemical Physics **98**, 6769 (1993); doi: 10.1063/1.464769
View online: http://dx.doi.org/10.1063/1.464769
View Table of Contents: http://aip.scitation.org/toc/jcp/98/9
Published by the American Institute of Physics

The effect of nonpolar solvents on Rydberg states: van der Waals complexes of azabicyclooctanes

Q. Y. Shang, P. O. Moreno,[a] C. Dion, and E. R. Bernstein
Colorado State University, Chemistry Department, Fort Collins, Colorado 80523

(Received 27 November 1992; accepted 20 January 1993)

The effect of solvation by nonpolar solvents on the $(n,3s)$ Rydberg states of 1,4-diazabicyclo[2.2.2]octane (DABCO) and azabicyclo[2.2.2]octane (ABCO) is investigated through mass resolved excitation spectroscopy of their van der Waals complexes. The solute/solvent clusters formed in a supersonic expansion include DABCO and ABCO with Ar, n-C_mH_{2m+2} $(m=1$–$7)$, and CF_4 and C_2F_6. The resulting spectra are analyzed with the help of empirical potential energy calculations of the cluster binding energies, minimum energy structures, van der Waals modes, and potential barriers between the various cluster minimum energy structures. Good agreement is found between the calculated and experimental results for DABCO and ABCO clustered with argon and methane. The spectra of clusters with all other hydrocarbons can be ascribed to only one major geometry for each cluster stoichiometry, despite the fact that calculations yield many stable geometries for each cluster. This apparent lack of agreement between calculations and experiments can be rationalized based on cluster binding energy, zero point energy, and the potential energy barriers between the cluster minima. The observed blue shift of the cluster 0_0^0 transition energy as a function of the n-alkane chain length can be qualitatively modeled by a Lennard-Jones potential for the solute–solvent interaction for both the ground and excited states. The model reveals a strong repulsive interaction between the Rydberg state electronic distribution and the solvent molecule. This repulsion depends on the distance between the solvent molecule and the solute molecule nitrogen atom.

I. INTRODUCTION

The study of electronic transitions of solute–solvent van der Waals clusters has focused on $n\pi^*$ and $\pi\pi^*$ valence states.[1] The spectra of such clusters combined with models of the solute–solvent interaction energy have led to a characterization of cluster geometry, binding energy, van der Waals vibrational modes, and the intermolecular potentials between the molecules comprising the cluster. These empirical potential models describe short-range solute–solvent and solvent–solvent interactions by classical potential functions which include dispersion, repulsion, Coulombic, charge transfer, and hydrogen bonding terms.[2] The parameters of these potentials are often obtained (for ground state systems) through fitting crystallographic and thermodynamic results. Comparison of spectroscopic results with those based on model potentials provides a critical test of the validity of the potential itself.[3]

A relatively small red shift of the origin transition (decreased transition energy) is often observed for valence transitions of nonpolar solute–solvent clusters. The cluster red shift in transition energy implies a larger solute–solvent binding energy in the excited state than the ground state. The increased excited state cluster binding energy can be attributed to an increase in the solute polarizability upon electronic excitation which increases the dispersion interaction between the solute and solvent molecules in the cluster. Little change is expected for the exchange repulsion interactions upon electron excitation within the valence shell because the transition involves changes in the phase of the electronic wave functions only, while the extent of the electronic distribution remains relatively unchanged.[4]

For clusters comprised of polar solvents and various solutes, valence transitions (e.g., $n^2 \rightarrow n\pi^*$, $\pi^2 \rightarrow \pi\pi^*$, etc.) are known to shift both red and blue with respect to those of bare solute molecules. In these instances, solute and solvent dipolar interactions play the dominant role in determining the transition energy.[5] Solvent–solute hydrogen bonding can cause such transitions to shift $\sim 10^3$ cm^{-1} if the solute acts as a hydrogen bond acceptor.[1]

We have recently discussed the effect of solvation on Rydberg excited states.[6,7] The Rydberg transition studied involves a $2p$ lone pair electron promoted to a state of higher principle quantum number [e.g., $(2p)^2 \rightarrow (2p3s)$]. These nonpolar solvation studies were carried out for clusters of 1,4-dioxane with various nonpolar solvents and 1,4-diazabicyclo[2.2.2]octane (DABCO, **1**) and azabicyclo[2.2.2]octane (ABCO, **2**) with argon. Dioxane has two lone pairs of $2p$ electrons centered on each oxygen atom and DABCO and ABCO have a single lone pair of electrons centered on each nitrogen atom. One would expect that the excited Rydberg $3s$ orbital is somewhat localized near its parent atom and that a solvent molecule located close to that atom would have a greater effect on the $(2p)^2 \rightarrow (2p3s)$ transition energy than one located at a more distant position. This reasoning is validated by both calculations and experiments. Such cluster structures for dioxane/nonpolar solvent are assigned and calculated and they can be distinguished by their cluster spectroscopic shifts.[6] A similar phenomenon is observed for the ABCO

[a]Present address: Dow Chemical Company, Freeport, TX 77541.

 0021-9606/93/096769-10$06.00 © 1993 American Institute of Physics

and DABCO/argon clusters.[7] A unique correlation emerges for the observed cluster origin shift of the $(2p)^2 \rightarrow (2p3s)$ Rydberg transition with the calculated DABCO and ABCO/argon cluster geometries. A large repulsive interaction is found for an argon atom located close to the nitrogen atom of DABCO and ABCO following excitation to the Rydberg state. Furthermore, for DABCO and dioxane, the experimental results support the conclusion that two chromophoric atoms (O and N) in both these molecules participate in the excitation. The excited $3s$ Rydberg orbital is delocalized over the entire framework of the molecules.

This paper reports the extension of the study of DABCO and ABCO Rydberg transitions in van der Waals clusters to nonpolar solvents other than argon. The additional solvent systems include n-C_mH_{2m+2} ($m=1,...,7$), CF_4, and C_2F_6. Cluster structures and binding energies are assigned for these systems based on the DABCO and ABCO/argon results and on calculations employing empirical potential energy functions. ABCO and DABCO/ethane or larger chain hydrocarbons clusters show only one obvious structure, while the ABCO and DABCO/fluorocarbon clusters evidence two or three unique geometries. Calculations for these systems generate a number of geometries for each cluster. The experimental and calculational results are rationalized based on zero point energies and the calculated cluster potential surface (i.e., barriers between calculated minima). Blue shifts for the cluster Rydberg transition origins ($R_{3s} \leftarrow S_0$) are found to be a function of chain length of the hydrocarbon. These studies shed light on the spatial extent of the repulsive interaction of the $3s$ Rydberg state electron configuration with the solvent molecule.

II. PROCEDURES

A. Experiment

Mass resolved excitation spectra (MRES) are obtained through one photon resonance enhanced multiphoton ionization and time of flight mass resolution. The detailed experimental design and procedures have been recently outlined.[8] Briefly the clusters of DABCO and ABCO with the various solvents are generated in a supersonic expansion through a pulsed nozzle. The vacuum system is maintained at 2×10^{-6} Torr during the experiment. A solid sample of either DABCO or ABCO is placed within the nozzle and heated to 50 °C for DABCO and 35 °C for ABCO. The expansion gas consists of 1%–5% solvent molecule and helium premixed in a high pressure tank. No special purification of any of the sample components is necessary since the spectra are mass resolved.

For DABCO clusters, the excitation laser is a doubled Nd/YAG pumped dye laser with fluorescence 548 (Exciton) in an alkaline methanol solvent as the active lasing medium. Ionization of the clusters with a second color near the threshold for ionization shows no fragmentation of larger clusters for any of the solute/solvent clusters.

For ABCO/nonpolar solvent clusters, the excitation laser output is generated by doubling and mixing (with 1.064 μm radiation from the Nd/YAG fundamental) the fundamental dye frequency. The dye laser operates with an active medium of a 1:3 mixture of DCM/LDS 698 in methanol.

The input laser beam is focused to the ionization/excitation point by a 35 cm lens. Cluster ion fragmentation is not a problem for these clusters as a comparison between one- and two-color MRES demonstrates for the various solvents and thus the reported data are obtained by one-color MRES techniques due to the higher signal to noise ratio for this technique. Signals for larger solvent molecule clusters are more intense than those for argon and methane due probably to the large binding energies for the former clusters and hence the higher cluster concentration in the expansion.

The negative peaks that appear in some of the cluster spectra are due to detector overload at the bare molecule and impurity mass channels.

B. Calculation

The ground state minimum energy cluster geometries are predicted by an empirical atom–atom potential of the Lennard-Jones–Coulomb (6-12-1) form.[9] The geometries and atomic charges of the isolated molecules composing the clusters are obtained through MOPAC 6 semiempirical calculations. Both charges and geometries are fixed throughout the cluster energy minimization procedure. Potential parameters are employed from the work of Scheraga.[10]

III. RESULTS

A. Calculated stable cluster geometries

The calculated stable geometries of DABCO and ABCO clustered with argon have been presented in a previous publication[7] and they are pictured in Fig. 1. These cluster structures serve as a foundation for expectations concerning other cluster geometries. Three types of geometries constitute stable potential energy minima for argon clusters—(type I) an argon atom located above the C_3 axis centered between two C–C bridges; (type II) an argon atom located above the N atom of ABCO or DABCO near the C_3 axis, but not on it; (type III) the argon atom near the C_3 axis at the CH position (tertiary carbon) of ABCO. These general structures are also found both by calculations and experiments for DABCO and ABCO/methane clusters. Empirical potential energy calculations for the structure of DABCO and ABCO clustered with larger n-alkanes (C_2 through C_7) are also explored. The major structural features of these latter clusters are quite similar to those of the DABCO and ABCO/argon and methane clusters—types I, II, and III cluster structures can still be recognized. The longer chain normal alkanes can additionally orient in different ways at each of the three ABCO and DABCO "binding sites." These "local orientational" structures may not be stable for the actual clusters created in the supersonic expansion for reasons associated with cluster binding energies, barriers to internal cluster motion, and zero point energies.

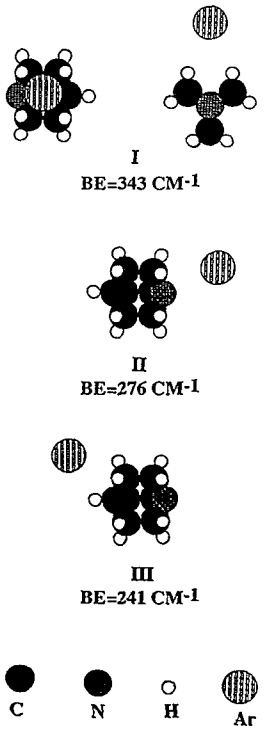

FIG. 1. A representation of the binding geometries for $ABCO(Ar)_1$ cluster based on the calculation with the classical model potential. Binding energies (BE) are presented in the figure for each structure. $DABCO(AR)_1$ has only geometries I and II. The binding energy presented for the clusters is calculated based on new argon parameters obtained from the spectroscopic results of Herman, LaRocque, and Stoicheff (Ref. 11). The new argon parameters are $\alpha=1.64\times10^{24}$ cm^3, $N=17.72$, and $rg=3.76$ Å (see Ref. 10 for a definition of the notations). Our previous calculations (Refs. 6 and 9) underestimated the argon parameters.

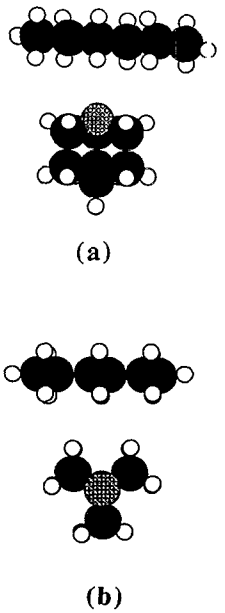

FIG. 2. A representation of the calculated geometrical arrangements for the two most stable cluster structures: (a) $ABCO(hexane)_1$ (type II); (b) $DABCO(hexane)_1$ (type I).

The most stable cluster geometry for ethane or longer chain hydrocarbon solvents associated with ABCO and DABCO is roughly type II, as depicted in Fig. 2. The plane determined by the heavy atom chain of the hydrocarbon is almost perpendicular to the C_3 axis of the solute. The second most stable geometry for larger chain hydrocarbon clusters with the solute molecules is a type I structure in which the *n*-alkane chain axis is nearly perpendicular to the C_3 axis of the solute (Fig. 2). Table I lists the binding energies of these two types of geometries for some representative systems. These results agree with the experimental data reported and discussed below.

B. MRES of DABCO/nonpolar solvent clusters

The mass resolved excitation spectra (MRES) of DABCO clustered with various solvents (Ar, CH_4, CF_4, C_2H_6, C_2F_6, C_3H_8, *n*-C_4H_{10}, *n*-C_5H_{12}, *n*-C_6H_{14}, and *n*-C_7H_{16}) are displayed in Fig. 3.

1. $DABCO(Ar)_1$

The spectrum of $DABCO(Ar)_1$ has been discussed previously.[7] Studies involving nozzle/laser timing delay and population depletion indicate that the spectrum derives from three sets of cluster structures. A set of sharp features to the low energy side of the spectrum at about 35 890 cm^{-1} is assigned to type I cluster geometry. A weak, somewhat broad peak at ~36 100 cm^{-1} belongs to type II cluster geometry and a very broad feature centered about 36 200 cm^{-1} is due to $DABCO(Ar)_2$ dissociation.

Cluster formation induces the molecule one-photon forbidden Rydberg transition origin to become allowed. The origin shift for the cluster with respect to the bare molecule is calculated as the difference between the one-photon origin of the cluster and the two-photon origin of the bare molecule. Type I cluster geometry thereby has a 104 cm^{-1} blue shift and type II geometry has a 290 cm^{-1} blue shift for the Rydberg transition. The sharp drop in signal for the type II origin feature at ~36 100 cm^{-1} is due to the onset of $DABCO(Ar)_1$ cluster dissociation. This signal is observed to rise in the bare molecule mass channel as it falls in the $DABCO(Ar)_1$ cluster mass channel. Dissociation is expected for this cluster based on the calculated binding energy for the ground state system.

We will base our interpretation of the spectra for the other clusters on the $DABCO(Ar)_1$ cluster calculational and experimental results.

TABLE I. The calculated binding energies (cm^{-1}) for two most stable geometries for 1:1 DABCO and ABCO clusters with various solvents (see Fig. 2).

	DABCO		ABCO	
Solvent	Type II	Type I	Type II	Type I
Ar	293	341	276	343
CH_4	375	405	380	406
C_2H_6	542	541	554	542
C_3H_8	717	677	733	683
n-C_6H_{14}	1074	989	1095	997

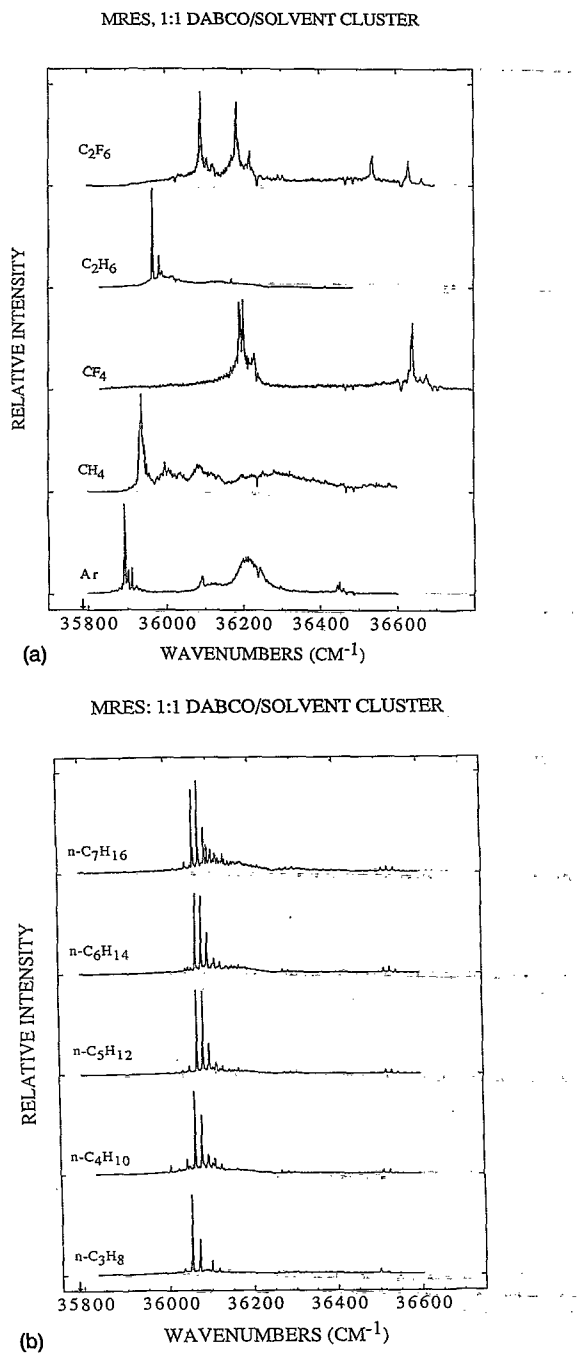

FIG. 3. One-photon MRES of the DABCO clusters in the region of the DABCO (n,3s) excited state. The cluster composition is determined from the flight time in TOF-MS. The arrow marks the position of the bare DABCO two-photon allowed origin transition.

2. DABCO(CH_4)$_1$

The spectrum of DABCO$(CH_4)_1$ is presented in Fig. 3(a). The first feature at the low energy end of the spectrum (35 935 cm^{-1}) is relatively sharp and blue shifted by 149 cm^{-1} from bare molecule's 0_0^0 transition. The width of this feature is due probably to unresolved low energy (rotational) van der Waals modes associated with CH_4 motion. Such congestion has also been observed for the Rydberg spectrum of dioxane/methane clusters.[6] This low energy feature can readily be correlated with a type I cluster spectrum as defined for DABCO$(Ar)_1$.

Three additional broad features can be identified in the DABCO$(CH_4)_1$ spectrum presented in the figure—these are centered at 36 000, 36 085, and 36 280 cm^{-1}. Their assignments can only be made qualitatively and through comparison with the DABCO$(Ar)_1$ results. For DABCO$(Ar)_n$ clusters, the assignments are supported by hole-burning/depletion experiments and calculations. Since the calculations for DABCO$(CH_4)_1$ clusters are so similar to those for DABCO$(Ar)_1$, the spectra of the DABCO$(CH_4)_1$ system are assigned in a similar fashion. van der Waals mode energies and intensities are comparable for both clusters. The feature at 36 085 cm^{-1} is $\sim$300 cm^{-1} shifted from the bare molecule origin and can thus be assigned as being due to a cluster with type II geometry (see Fig. 1). This cluster does not appear to dissociate. The absence of dissociation even for a cluster with such a large blue shifted absorption is due probably to the higher binding energy for the CH_4 cluster. The broad features at 36 280 cm^{-1} could be due to dissociation of DABCO$(CH_4)_2$ as it is similar to a comparable feature found for DABCO$(Ar)_2$ in the DABCO$(Ar)_1$ mass channel. The assignment of the broad features at 36 000 cm^{-1} is not clear. Its blue shift is too small for it to be associated with fragmentation of higher order clusters. This feature could be due to a van der Waals mode (65 cm^{-1}) of the DABCO$(CH_4)_1$ type I structure.

3. DABCO(CF_4)$_1$

The interest in the DABCO$(CF_4)_1$ cluster system lies in its similarity to the DABCO/methane system. We were hopeful that the spectrum of DABCO$(CF_4)_1$ would be useful in assigning the spectrum of DABCO$(CH_4)_1$. The two spectra are in fact different enough that the assignment of one has little to do with the assignment of the other.

The spectrum of DABCO$(CF_4)_1$ appears to be very different from that of DABCO$(CH_4)_1$ as can be seen in Fig. 3(a). The first set of peaks falls near 36 200 cm^{-1} and an additional set is found at $\sim$36 630 cm^{-1}. The first set of features could be assigned as being due to either type I or II cluster structures. The feature at $\sim$430 cm^{-1} to the blue of the origin is probably associated with an internal vibration of the bare molecule.

4. DABCO(C_2H_6)$_1$

The spectrum of DABCO$(C_2H_6)_1$ appears to be quite simple [Fig. 3(a)]. The first sharp peak at 35 966 cm^{-1} is 180 cm^{-1} to the high energy side of the bare molecule 0_0^0 transition. The feature is assigned to the 0_0^0 transition of the type I cluster structure of DABCO$(C_2H_6)_1$. The three features which appear to be built on the origin lie at 16, 23, and 50 cm^{-1} to the blue of it—they are assigned as transitions due to van der Waals vibrations. Two additional weak features appear at 203 and 448 cm^{-1} to the blue of the 0_0^0 transition—these can be associated with transitions to internal excited state vibrational modes of the bare mol-

TABLE II. The transition origins and relative shifts (cm^{-1}) with respect to the bare molecule for the 1:1 clusters of DABCO and ABCO with various solvents. The DABCO cluster is assigned as type I geometry and the ABCO cluster is assigned as type II geometry.

	DABCO		ABCO	
Solvent	Origin	Relative shift	Origin	Relative shift
...	35 786	...	39 102	...
argon	35 891	105	39 332	230
methane	35 935	149	39 377	275
ethane	35 966	180	39 474	372
propane	36 053	267	39 644	542
n-butane	36 064	278	39 665	563
n-pentane	36 072	286	39 683	581
n-hexane	36 070	284	39 689	587
n-heptane	36 065	279	39 691	589

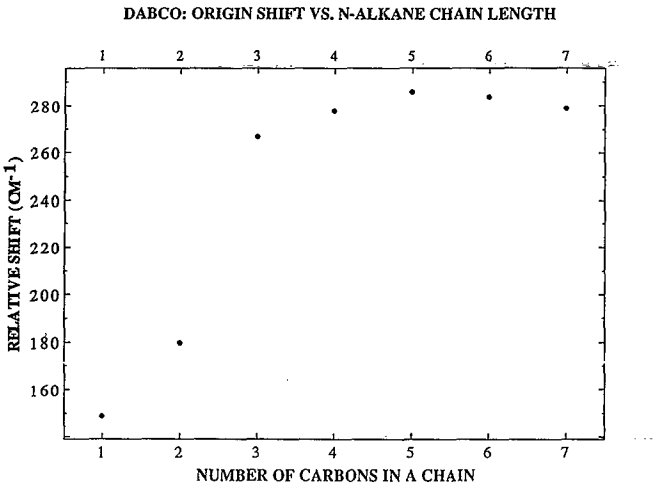

FIG. 4. A plot of the origin shift as a function of the *n*-alkane chain length for the DABCO cluster. *n* is the number of the carbon atoms in the chain.

ecule.[7] These two excited state vibrational modes of DABCO can be associated with those found for all other DABCO/*n*-alkane clusters. No feature in this spectrum can be associated with type II cluster structure identified for DABCO$(Ar)_1$ and $(CH_4)_1$ (see Fig. 1).

5. DABCO$(C_2F_6)_1$

The spectrum of DABCO$(C_2F_6)_1$ is presented in Fig. 3(a). The first peak in this spectrum at 36 091 cm^{-1} is a 0_0^0 transition for the cluster—it is blue shifted 305 cm^{-1} from the bare molecule origin. At least two cluster van der Waals features appear at 8 cm^{-1} intervals built on the cluster origin. An additional set of features appears at a blue shift of 397 cm^{-1} from the bare molecule origin, or 92 cm^{-1} from the first cluster feature. Possible assignments for this latter feature are (1) a cluster mode built on the origin, or (2) a new cluster origin associated with a type II cluster structure. Both of these features have an internal mode at 447 cm^{-1} built on them.

6. DABCO$(n-C_mH_{2m+2})_1$, $m=3,...,7$

The spectra of DABCO/*n*-alkane clusters for *n*-alkanes with three to seven carbon atoms ($m=3,...,7$) are all quite similar to one another. The individual spectra are displayed in Fig. 3(b). The first intense feature in each spectrum is assigned as an origin for the cluster. The features to the low energy side of this origin are assigned as hot bands and reflect transitions from ground electronic state van der Waals modes. The origin energies are 36 053, 36 064, 36 072, 36 070, and 36 065 cm^{-1} for $m=3$–7, respectively. The van der Waals vibrational intervals built on these origins are all roughly 15 cm^{-1}. The two internal modes of DABCO at 203 and 448 cm^{-1} from the 0_0^0 transition are also observed. By comparison with Ar and CH_4/DABCO clusters, these transitions must be associated with type I cluster structure (see Table II). Clusters with type II structure are apparently not observed.

To summarize these results, two types of structures (I and II of Fig. 1) are found for the DABCO$(Ar)_1$ cluster by both experiments and calculations. A similar identification can be made for DABCO$(CH_4)_1$ clusters. Only type I cluster structures are found for DABCO/*n*-alkane, $m=2,...,7$ clusters. The two perfluoroalkane solvents studied, CF_4 and C_2F_6, have spectra which cannot be readily fit into this structural scheme. The results for the cluster transition origin shifts are tabulated and plotted in Table II and Fig. 4. As the figure shows, the cluster blue shift increases rapidly with hydrocarbon chain length from methane to propane then slowly from propane to heptane. The blue shift reaches a saturation value at *n*-pentane and essentially remains constant as *m* increases. This result reflects the spatial extent of the Rydberg orbital and will be discussed below in Sec. IV.

C. MRES of ABCO/nonpolar solvent clusters

The same cluster series has been explored for the ABCO Rydberg chromophore as reported above for DABCO. These spectra are displayed in Figs. 5(a) and 5(b). The Rydberg transition for ABCO and its clusters is one photon allowed and the bare molecule transition $(2p)^2 \rightarrow (2p3s)$ lies at 39 102 cm^{-1}.

1. ABCO$(Ar)_1$

The spectrum of ABCO$(Ar)_1$ has been assigned previously.[7] Based on a comparison with the DABCO$(Ar)_1$ cluster spectrum, one can suggest that transitions associated with a new cluster geometry appear in the spectrum. The new structure is predicted by the empirical potential models discussed above. The type III geometry of Fig. 1, with the argon atom near the tertiary carbon, off the C_3 axis, is suggested because the new cluster feature is red shifted (28 cm^{-1}) from the isolated molecule origin and the feature only appears for the ABCO system. The feature at 39 148 cm^{-1} (blue shifted by 46 cm^{-1} from the ABCO 0_0^0 transition) is assigned to a type I structure. A type II structure cluster is assigned to the broad feature commen-

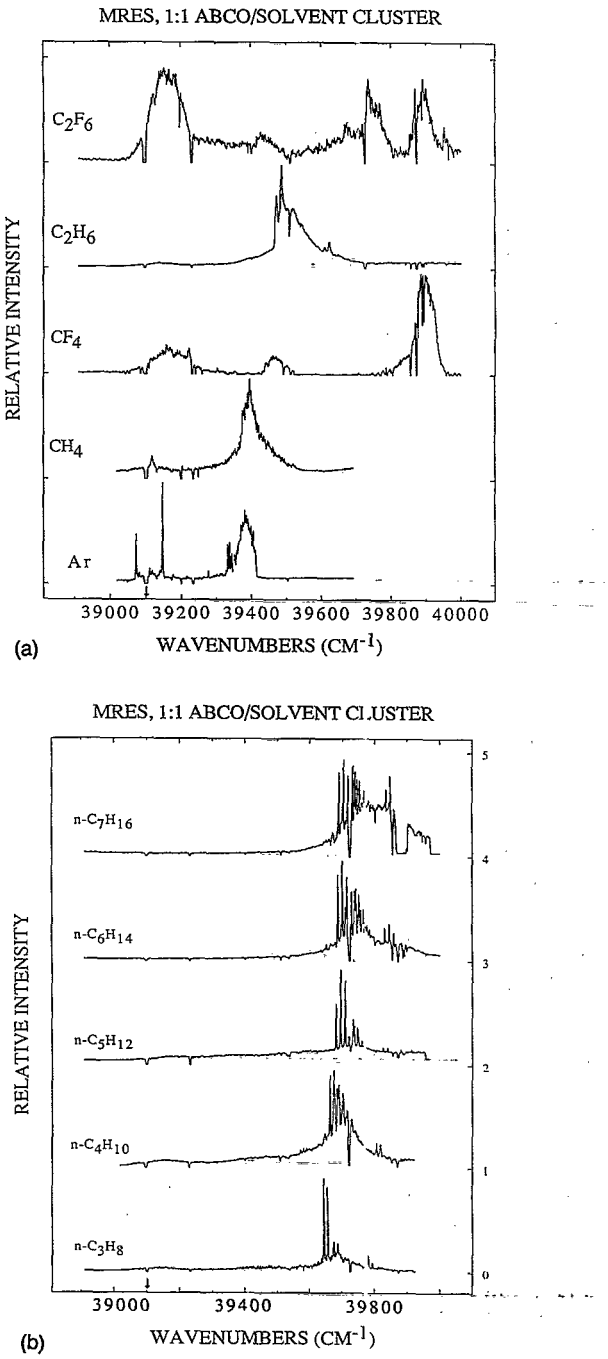

FIG. 5. One-photon MRES of the ABCO clusters in the region of the ABCO (n,3s) excited state. The cluster composition is determined from the flight time in TOF-MS. The arrow marks the position of the bare ABCO one-photon allowed origin transition.

cing at 39 332 cm^{-1}. The onset of this feature is blue shifted by 230 cm^{-1} from the bare molecule origin.

2. ABCO(CH$_4$)$_1$

The spectrum of ABCO$(CH_4)_1$ shows a major broad feature starting at 39 377 cm^{-1} [Fig. 5(a)]. Based on a comparison with the foregoing ABCO$(Ar)_1$ system, this feature is assigned as arising from an ABCO$(CH_4)_1$ type II structure cluster. Unlike the argon system, no abrupt drop in signal at the higher energy side of this feature is found and thus the ABCO$(CH_4)_1$ cluster is more tightly bound in the Rydberg state than the ABCO$(Ar)_1$ cluster in this geometry. No features are found for this cluster that can readily be assigned as arising from type I and III geometries. Two other weak features can be identified in the ABCO$(CH_4)_1$ spectrum—one is a slightly broadened peak with an 18 cm^{-1} blue shift ($\sim$39 120 cm^{-1}) from the ABCO origin and the other is a $\sim$150 cm^{-1} wide feature between 39 050 and 39 200 cm^{-1}. The former feature might be associated with a cluster with type I geometry and the latter, since it begins to the red of the origin, could be due to a type III geometry cluster. Further support for these tentative assignments comes from the spectrum of the ABCO$(CF_4)_1$ cluster system.

3. ABCO(CF$_4$)$_1$

The spectrum of the ABCO$(CF_4)_1$ clusters is presented in Fig. 5(a). It consists of three main broad features. The many sharp negative features arise from detector saturation and coincide with the ABCO isolated molecule transitions[7] and additional (unknown) impurities in the sample. The ABCO bare molecule signals are roughly 500 times more intense than the cluster signals. The lowest energy one of the three broad features extends to the red of the bare molecular 0_0^0 transition, the next feature is at +310 cm^{-1} from the ABCO origin, and the highest energy feature lies at +700 cm^{-1} from the bare molecule 0_0^0. We assign these features, respectively, to type III, type I, and type II geometry cluster origins of the ABCO$(CF_4)_1$ cluster system based on the ABCO$(Ar)_1$ results. These results and assignments lend support to the assignment of the weak features found for ABCO$(CH_4)_1$.

4. ABCO(C$_2$H$_6$)$_1$

The spectrum of ABCO$(C_2H_6)_1$ presented in Fig. 5(a) shows a set of intense peaks starting at 39 474 cm^{-1}, 372 cm^{-1} blue shifted from the bare ABCO origin. In comparison with the spectra of ABCO$(Ar)_1$ and $(CH_4)_1$, the size of this shift suggests assignment of this feature to a type II cluster structure. The second sharp feature in this set is 13 cm^{-1} from the first and is due probably to a transition to a van der Waals mode of the cluster. These two sharp features are repeated at +136 cm^{-1} from the cluster origin—the 136 cm^{-1} mode is an internal vibration of the bare ABCO molecule. The weak broad feature extending to the red of the bare molecule origin is due probably to a cluster with type III structure. A similar feature is assigned for ABCO$(CH_4)_1$.

5. ABCO(C$_2$F$_6$)$_1$

The spectrum of ABCO$(C_2F_6)_1$ is similar to that found for ABCO$(CF_4)_1$ and it consists of three prominent broad features. These features can be assigned as the ABCO$(CF_4)_1$ cluster spectrum is assigned. The first feature is

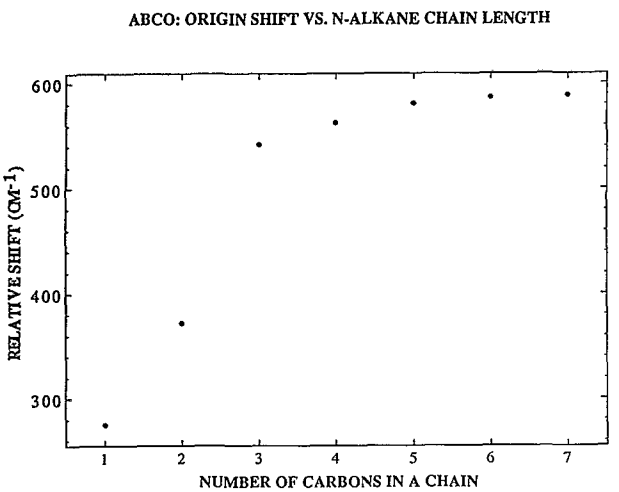

FIG. 6. A plot of the origin shift as the function of the *n*-alkane chain length for the ABCO cluster. *n* is the number of the carbon atoms in the chain.

assigned to a cluster of type III structure, the feature at $+581$ cm^{-1} from the ABCO origin is assigned to a cluster of type I structure, and the feature at $+715$ cm^{-1} from the ABCO origin is assigned to a cluster of type II structure.

6. ABCO(n-alkane)$_1$, $m=3,...,7$

The spectra of ABCO(*n*-alkane)$_1$, $m=3,...,7$ clusters are very similar to each other and the comparable DABCO/*n*-alkane clusters as well. The first strong features in these spectra lie at 39 644, 39 664, 39 683, 39 689, and 39 691 cm^{-1} for $m=3$–7, respectively. The sharp, weak features just to the red of these origin transitions can be assigned as a van der Waals hot band transition. Again the intervals for the progressions are all roughly 13 cm^{-1}. The complexity and congestion in these spectra increase as the *n*-alkane becomes longer. An internal mode at 136 cm^{-1} can also be detected in these spectra. The cluster responsible for these features is most likely of type II structure. This preliminary assignment is made through comparison with the shifts of the other ABCO clusters reported above. Only very faint features appear near the ABCO bare molecule origin that can be ascribed to a type III cluster structure. No features associated with type II structures can be identified.

To summarize these results for ABCO clusters, three geometries of clusters are identified for the ABCO(Ar)$_1$ cluster. The spectra of ABCO clustered with *n*-alkanes evidences only one distinct geometry which can be assigned as type II. Type III geometry clusters of methane and ethane yield weak, broad, red shifted cluster spectral features. This assignment is supported by the perfluoroalkane cluster spectra. The presence of type I structure cluster spectra in the ABCO/hydrocarbon cluster systems is not obvious.

Table II lists the origins of type II geometry ABCO clusters based on the above assignments and Fig. 6 displays a plot of the spectral shifts as a function of *n*-alkane chain length. The shift clearly saturates near *n*-pentane. Similar behavior is identified for DABCO clusters; however, DABCO clusters seem to adopt a type I geometry (small shift), while ABCO clusters adopt a type II geometry (large shift).

IV. DISCUSSION

A. Cluster geometries

As can best be noted from the ABCO(Ar)$_1$ system [Fig. 5(a)], three stable solvation sites can be identified for an ABCO molecule. This conclusion is confirmed by calculations (Fig. 1)—type I geometry has the argon atom above the C_3 axis of ABCO centered between two of the three bridge (CH_2–CH_2) groups of the molecule, type II geometry has the argon atom near the nitrogen atom of ABCO just off the C_3 axis above the CH_2–N–CH_2 "triangle," and type III geometry has roughly the same configuration as type II geometry, but the argon is positioned at the tertiary carbon end of the ABCO molecule. This latter geometry is only present for ABCO as a unique structure.[7]

Since the $3s \leftarrow 2p$ excitation of the nitrogen lone pair electron is expected to be localized in the vicinity of the nitrogen end of ABCO, the argon atom nearest the nitrogen should exert the largest effect on the transition energy. Thus the cluster transition shift is greatest for type II geometry clusters. Figure 5(a) shows an ABCO(Ar)$_1$ broad feature blue shifted 230 cm^{-1} from the ABCO origin due to type II structure clusters. The feature blue shifted at 46 cm^{-1} from the ABCO 0_0^0 transition must be due to a type I structure and the feature that displays the red shift[7] is assigned as being due to a type III structure ABCO(Ar)$_1$ cluster. For α DABCO(Ar)$_1$ cluster, type I and III structures are equivalent and only two origin transitions are observed from type I and II clusters.

While the argon cluster system seems to be straightforward with all stable sites equally occupied, the other ABCO and DABCO/solvent clusters do not appear to be so systematic. Calculations suggest that CH_4 clusters should adopt the same geometries as Ar clusters, but that the binding energies should be roughly twice as large. Similar trends obtain both experimentally and calculationally for aromatic systems.[1] The features in the CH_4 cluster spectra can be correlated with the calculated geometries even if the width and intensity of some of the features are not clearly understood. For hydrocarbons other than methane, the three main classifications of structures are still found, but many more specific site structures are calculated than are observed. As can be seen in Figs. 3(a) and 3(b) and 5(a) and 5(b), far fewer structures are observed than are calculated. In fact, even the existence of the main structure types (i.e., I, II, and III of Fig. 1) is not always evident in the spectra of ABCO and DABCO/hydrocarbon clusters. Only one structure type (I for DABCO and II for ABCO) plus van der Waals modes is evident for each cluster system.

Orientation of the solvent at the main solvation sites

may only be separated by small energy barriers and the zero point energy of the cluster system may be too large for the solvent to be trapped in a specific local orientation. Such a mechanism has also been suggested for ABCO and DABCO$(Ar)_1$ clusters to explain the absence of extra "local orientations" at type I sites. In this latter case, stable points are calculated for a type I structure with Ar above a CH_2–CH_2 bridge and between two CH_2–CH_2 bridges (Fig. 1). The barrier between the two wells in this instance is 20 cm^{-1}. For the more orientationally complex systems, the barriers are similar (<100 cm^{-1}), but more difficult to calculate.

In addition, the cluster formation process may further reduce the number of observed stable solvation sites for the ABCO and DABCO/hydrocarbon clusters. As the hydrocarbons become longer, the interaction between solute and solvent becomes larger and clusters begin to form with more internal energy. These hot clusters are much more likely to settle into their global energy minima than are cold clusters. Thus, the clustering process itself can also be responsible for generating only one stable geometry type rather than all three.

Calculations predict that as chain length increases, type II structures become more stable than type I structures. The experimental results for ABCO agree with this trend, but those for DABCO do not.

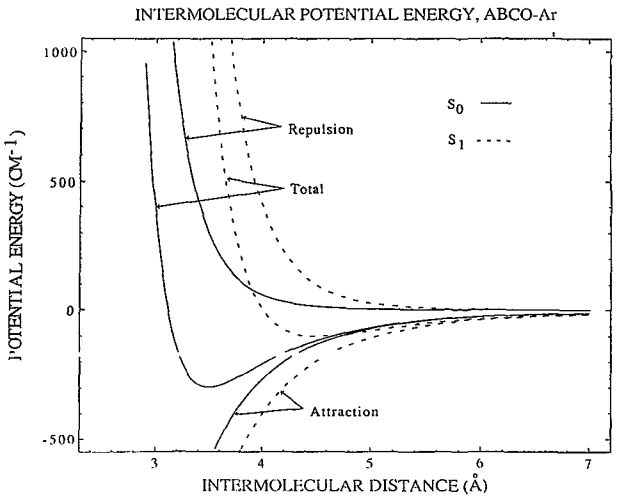

FIG. 7. Potential energy curves of argon interacting with the ABCO molecule based on the Lennard-Jones model. The solid curves represent the ground state and the dotted curve represents the $(n,3s)$ excited state of ABCO. The intermolecular distance is from the argon atom to the nitrogen atom of ABCO. The derivation of the parameters for plotting these curves is discussed in the text.

B. Rydberg electron/solvent interaction

The transition energy for the Rydberg state is blue shifted with respect to that of the bare molecule for both type I and II cluster structures. The increase in the transition energy for the cluster is due to the reduced binding energy for the cluster in the excited $(2p3s)$ Rydberg state with respect to the ground state. The interaction between nonpolar solvents and DABCO and ABCO is mainly of a van der Waals nature. One can model the difference between ground and excited state interactions with potential parameters that can be estimated from these experiments.

If solute and solvent molecules are considered to be two rigid spheres, the interaction between them can be modeled by a Lennard-Jones potential function

$$V(r) = -A/r^6 + B/r^{12}, \tag{1}$$

in which r is the distance between the solute and solvent. A and B are parameters of the attractive and repulsive parts of the potential, respectively. For the ground state, the parameters A and B can be calculated from a knowledge of the cluster binding energy and the equilibrium solute–solvent distance. The experimental binding energy for ABCO$(Ar)_1$ is ~ 300 cm^{-1} and the calculated equilibrium separation is ~ 3.5 Å (Ar–N distance) for the type II geometry cluster.

The experimental binding energy for the excited state cluster can be calculated from the difference between the dissociation energy and the onset energy of the Franck–Condon distribution of the broad peak for type II geometry clusters [39 320–39 420 cm^{-1} in Fig. 5(a)].[6,7] This excited state cluster binding energy is ~ 100 cm^{-1}. An additional piece of data is required to calculate the excited state potential parameters. The intermolecular solute–solvent separation is not easy to ascertain directly for the excited state.

The excited state separation, needed to complete the data set for evaluation of A and B for the excited state potential, can be estimated based on the excited state polarizability. The attractive part of the potential (A parameter) is directly proportional to the polarizabilities of the two centers involved. The polarizability of the Rydberg excited state is much larger than that of the ground state. Assuming that the attractive part of the excited state potential is 1.5 times that of the ground state, and using a binding energy of 100 cm^{-1} and $A_{Ryd} \sim 1.5\ A_0$, the potential function for the excited state can then be calculated and decomposed into repulsive and attractive parts. Figure 7 presents such plots for both ground and excited state potentials.

The decrease in the binding energy for the excited Rydberg state compared to ground state has been suggested to be due to an increase in the repulsive interaction with the solvent.[4] Figure 7 demonstrates this point quantitatively. The decrease in the excited state binding energy is due to the large increase in the repulsive part of the solute–solvent potential. This leads to an increase in the excited state solute–solvent separation of nearly 1.0 Å (3.5–4.5 Å) under the assumption made above ($A_{Ryd} \sim 1.5\ A_0$).

The increase in the repulsive interaction for the $3s$ excited Rydberg state compared with that for the ground state can be understood qualitatively. The expansion of the Rydberg orbital in the transition from a $(2p)^2$ to a $(2p3s)$ electronic configuration increases the overlap of the Rydberg orbital electron with the closed shell electron distribution of the solvent. The Pauli exclusion principle dictates

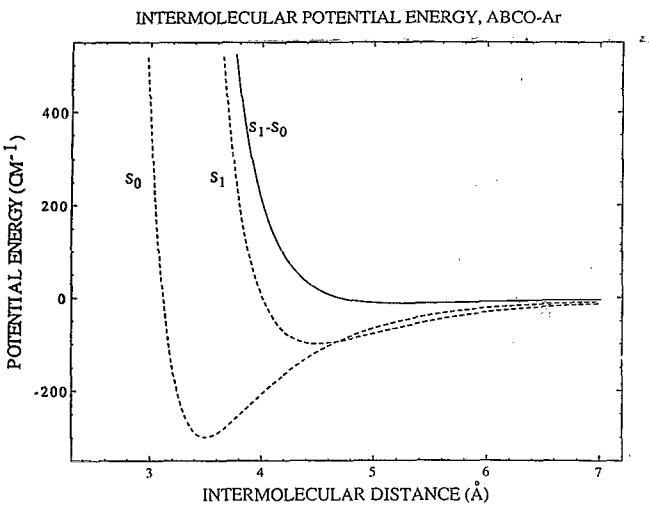

FIG. 8. Difference curve (solid) of the potential energy curves (from Fig. 7) of argon interacting with ABCO between the ground state $(2p)^2$ and the excited state $(2p3s)$. The solid curve represents argon interacting with the $(2p3s)$ Rydberg electron. The intermolecular distance is from the argon atom to the nitrogen atom of ABCO.

a repulsive interaction under such conditions. The increased separation of the solute and solvent due to this repulsion additionally lowers the attractive interaction.

If one assumes that the solute/solvent interaction for the rest of the molecule remains roughly constant upon Rydberg excitation, then subtraction of the ground state potential energy from the excited state potential energy at each separation distance represents the interaction of the Rydberg electron in the $3s$ orbital with the solvent. This prescription is presented in Fig. 8 for $ABCO(Ar)_1$. The intermolecular distance is taken from the Ar atom to the N atom of ABCO. The interaction between the $3s$ Rydberg orbital electron and Ar is clearly repulsive.

Consider the application of this model, as described above and in Figs. 7 and 8 for the type II cluster structure, to type I and III structures. The potential parameters employed for the type II structure analysis can be used for the other structures as well. The $(S_1–S_0)$ curve of Fig. 8 represents the blue shift of the $ABCO(Ar)_1$ spectrum as a function of distance between the N atom of ABCO and the Ar solvent atom. Type II geometry is calculated to have a 3.5 Å distance and a 230 cm^{-1} blue shift, type I geometry is calculated to have a 4.5 Å distance and a 18 cm^{-1} blue shift, and type III geometry is calculated to have a 6.2 Å distance and a 10 cm^{-1} red shift. These correlations are qualitatively correct and systematic, and help one think about the repulsive nature of the Rydberg state solvent interaction as a function of solvent and solvent–nitrogen separation. The blue shift for type I geometry of $DABCO(Ar)_1$ is 104 cm^{-1} [rather than 18 cm^{-1} for $ABCO(Ar)_1$] because the Rydberg orbital of DABCO is more diffuse than that of ABCO and thus it interacts more strongly with site I in these clusters.

We can also apply this model to aid in understanding the blue shifts of the DABCO and $ABCO(n\text{-alkane})_1$ cluster origins. $ABCO(CH_4)_1$ and $ABCO(Ar)_1$ are directly comparable with one another since similar calculations and experiments are found for both systems. One can then make the approximation that the Ar/solute molecule parameters also hold for each CH_3 or CH_2 group in the *n*-alkane chain. With these approximations, the blue shift for each cluster can be rationalized. The calculated geometry for the $ABCO(C_6H_{14})_1$ cluster is taken as an example (see Fig. 2). The distance of each carbon atom from the nitrogen atom is C_1—4.3 Å, C_2—3.6 Å, C_3—3.5 Å, C_4—3.6 Å, C_5—4.2 Å, and C_6—5.0 Å. The distance between N and C_3 is roughly the distance between C and N in an $ABCO(CH_4)_1$ cluster; the distance between N and C_3 and C_4 is close to that for ethane, etc. Assuming the shift is additive for each CH_2 group, the shifts thus predicted for the *n*-alkanes are thereby qualitatively reproduced by the distance/blue shift scale generated in Fig. 8. Moreover, this simple model also predicts the shift saturation effect displayed in Figs. 4 and 6. A similar correlation can be generated for $DABCO(C_6H_{14})_1$ (see Fig. 2).

This model is crude, but it does follow the essential features of the experimental results. The blue shifts of the $S_1 \leftarrow S_0$ transition for ABCO/*n*-alkane and DABCO/*n*-alkane solvent clusters can be derived from the $S_1–S_0$ curve in Fig. 8. The interactions of the Rydberg electron with solvent molecules appear to be more or less independent of the other valence electrons of the cluster. This Rydberg electron distribution is mostly centered on the N atom of ABCO.

V. CONCLUSIONS

The MRES of the nitrogen atom $[(2p3s) \leftarrow (2p)^2]$ Rydberg transition of ABCO and DABCO clusters with the nonpolar solvents Ar and *n*-alkanes $(m=1,...,7)$ are obtained and analyzed. Multiple geometries are observed for Ar and CH_4 clusters. Empirical potential energy calculations for cluster geometries and binding energies are in good agreement with the experimental findings for the two clusters. The blue shifts of the cluster transitions with respect to the isolated molecule correlates well with the cluster geometry. For *n*-alkane solvents, the observed cluster shifts are a smooth function of chain length. Only a single cluster structure can be assigned for *n*-alkanes C_2H_6 to C_7H_{16}. This result can be rationalized based on cluster binding energy, potential surface barriers between geometrically similar structures, and zero point motion.

A qualitative model is proposed to account for the behavior of the *n*-alkane cluster transition blue shift with increasing chain length. The model is based on the ABCO and DABCO/Ar cluster systems. It assumes that each CH_3 or CH_2 group of the alkane contributes to the shift as an Ar atom would, and that the blue shift of the Rydberg transition caused thereby is related to the distance between the ABCO and DABCO N atom and the O atom in the *n*-alkane. This model accounts for both the increased blue shift with increasing chain length and the saturation of the blue shift at pentane.

ACKNOWLEDGMENT

Supported in part by a grant from ARO-D.

[1] E. R. Bernstein, in *Atomic and Molecular Clusters*, edited by E. R. Bernstein (Elsevier, New York, 1990), p. 551.
[2] M. J. Ondrechen, Z. Berkovitch-Yellin, and J. Jortner, J. Am. Chem. Soc. **103**, 6586 (1981).
[3] F. A. Momany, R. F. McGuire, A. W. Burgess, and H. A. Scheragea, J. Phys. Chem. **79**, 2361 (1975).
[4] M. B. Robin and N. A. Kuebler, J. Mol. Spectrosc. **33**, 274 (1970).
[5] Q. Y. Shang and E. R. Bernstein, J. Chem. Phys. **97**, 60 (1992).
[6] P. O. Moreno, Q. Y. Shang, and E. R. Bernstein, J. Chem. Phys. **97**, 2869 (1992).
[7] Q. Y. Shang, P. O. Moreno, and E. R. Bernstein, J. Chem. Phys. (in press).
[8] E. R. Bernstein, K. Law, and M. Schauer, J. Chem. Phys. **80**, 207 (1984).
[9] S. Li and E. R. Bernstein, J. Chem. Phys. **95**, 1577 (1991).
[10] G. Nemethy, M. S. Pottle, and H. A. Scheraga, J. Phys. Chem. **87**, 1883 (1983).
[11] P. R. Herman, P. E. LaRocque, and B. P. Stoicheff, J. Chem. Phys. **89**, 4535 (1988).